

Figure S1. TEM images of CuCoMnO_x-200 (a), CuCoMnO_x-300 (b), CuCoMnO_x-400 (c) and CuCoMnO_x-500 (d).

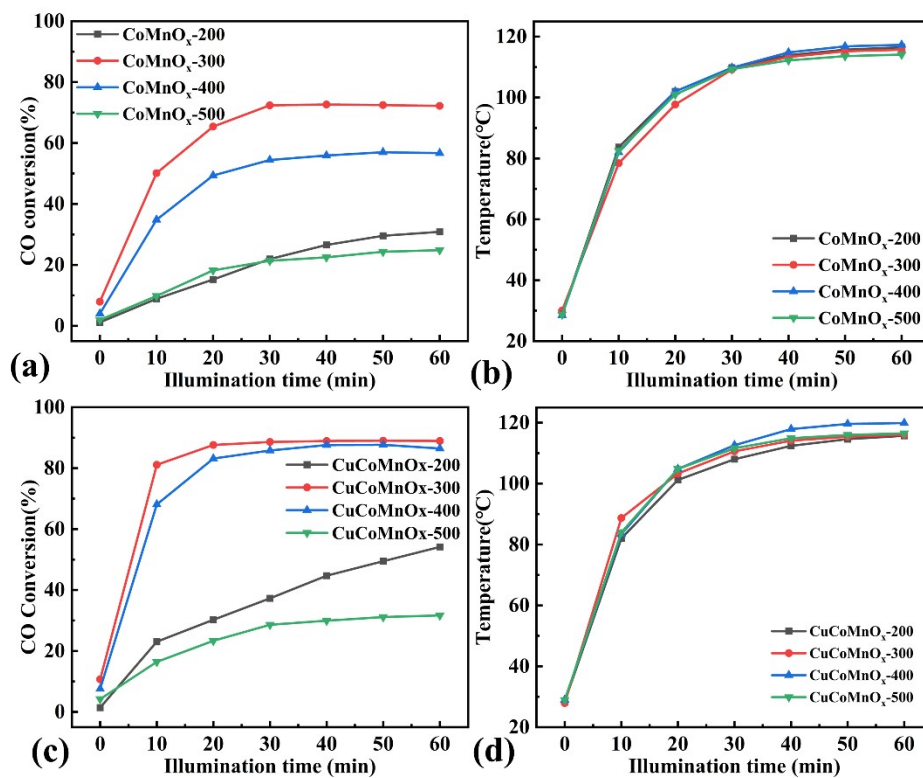


Figure S2. CO conversion (a,c) and temperature (b,d) curves of CoMnO_x-T and CuCoMnO_x-T in CO-PROX at 250 mW/cm².

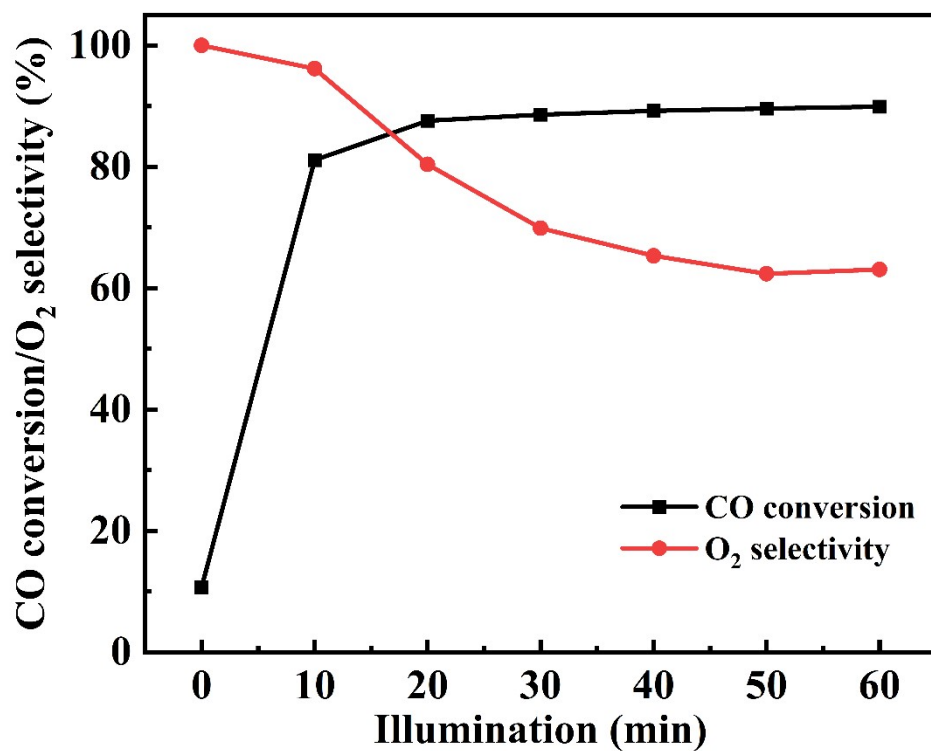


Figure S3. CO conversion and O₂ selectivity of CuCoMnO_x-300 for photothermal CO-PROX.

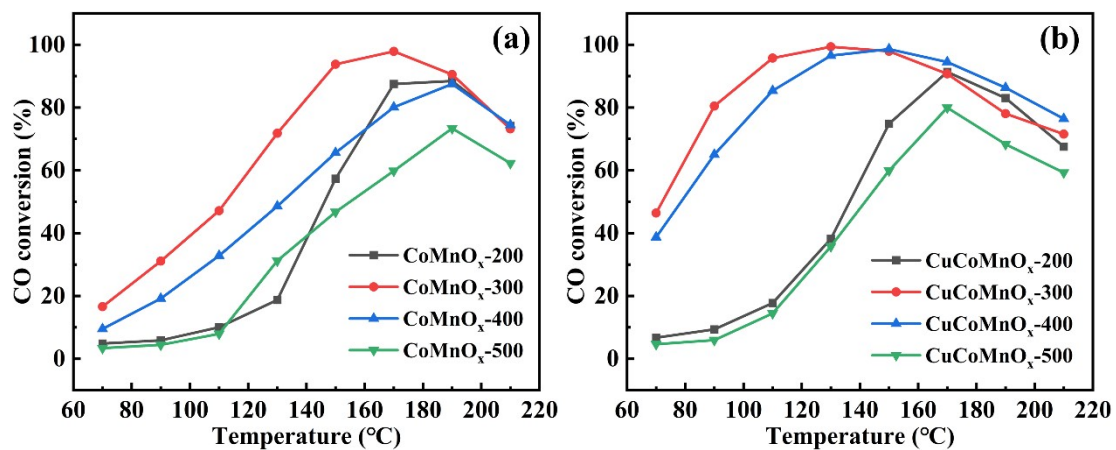


Figure S4. CO conversion of thermal catalysis over CoMnO_x-T (a) and CuCoMnO_x-T (b).

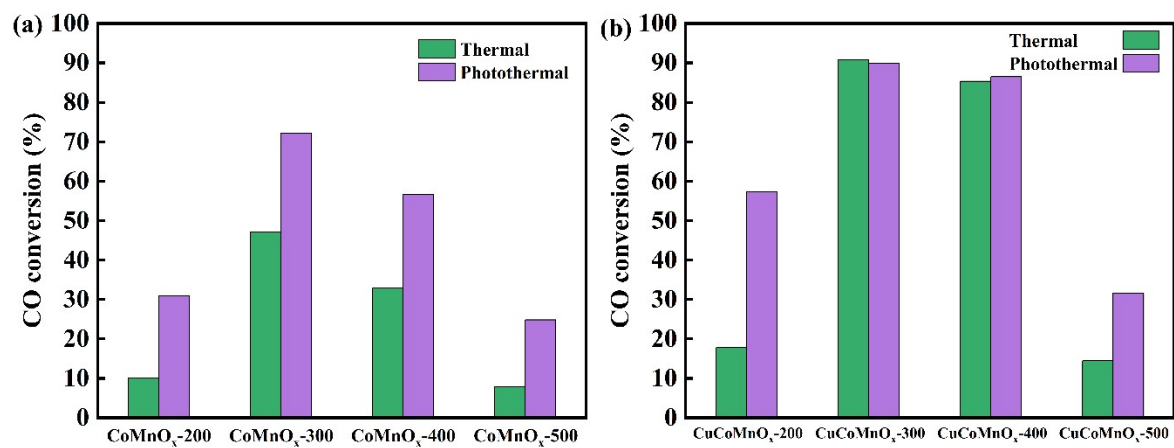


Figure S5. comparison of CO conversion of the CoMnO_x and CuCoMnO_x catalysts for thermal and photothermal CO-PROX.

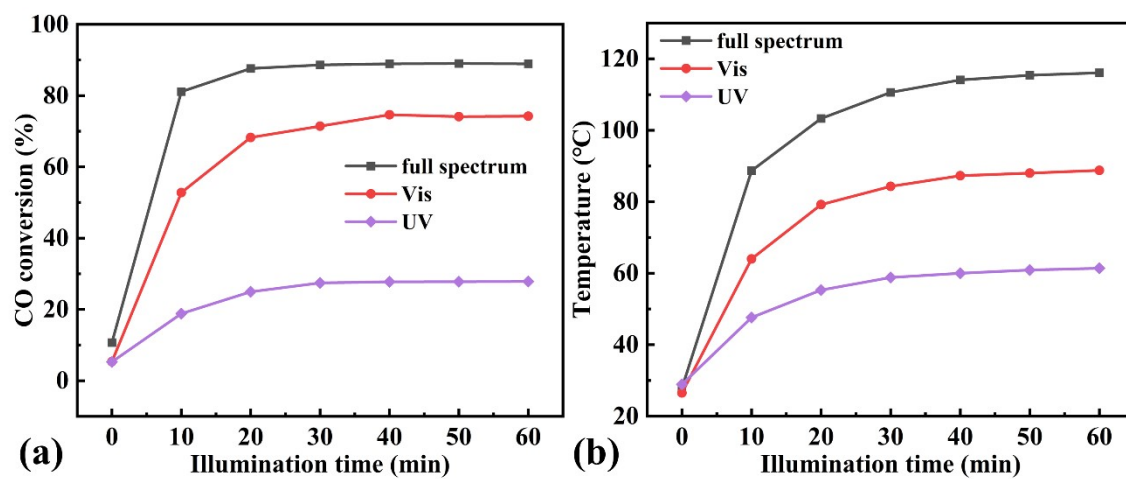


Figure S6. CO conversion and temperature curve of CuCoMnO_x-300 in CO-PROX at 250mW/cm² illuminated under different optical composition.

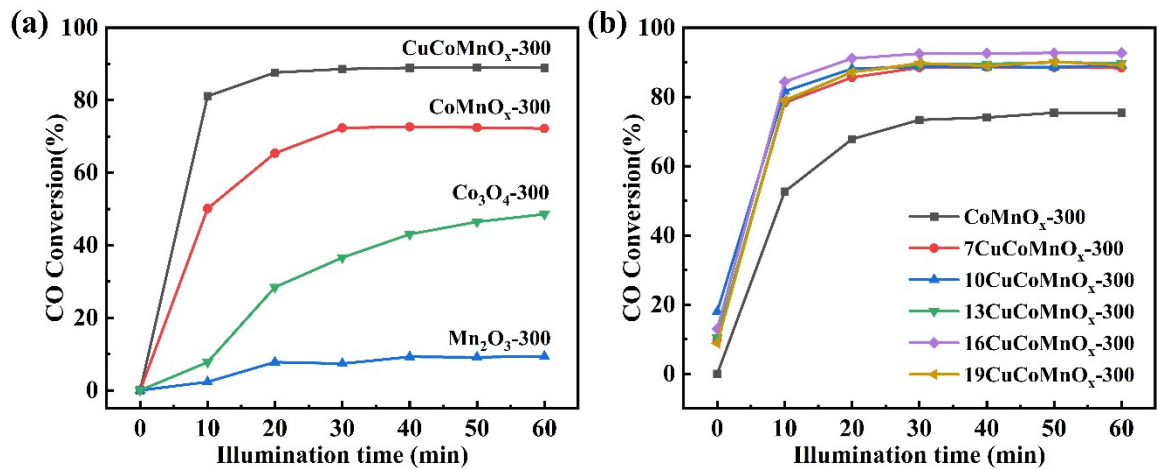


Figure S7. CO conversions of pure Co_3O_4 and Mn_2O_3 , binary CoMnO_x and ternary CuCoMnO_x calcined at $300\text{ }^\circ\text{C}$ (a) and CO conversions of CuCoMnO_x -300 with different copper amount in photothermal CO-PROX at $250\text{mW}/\text{cm}^2$.

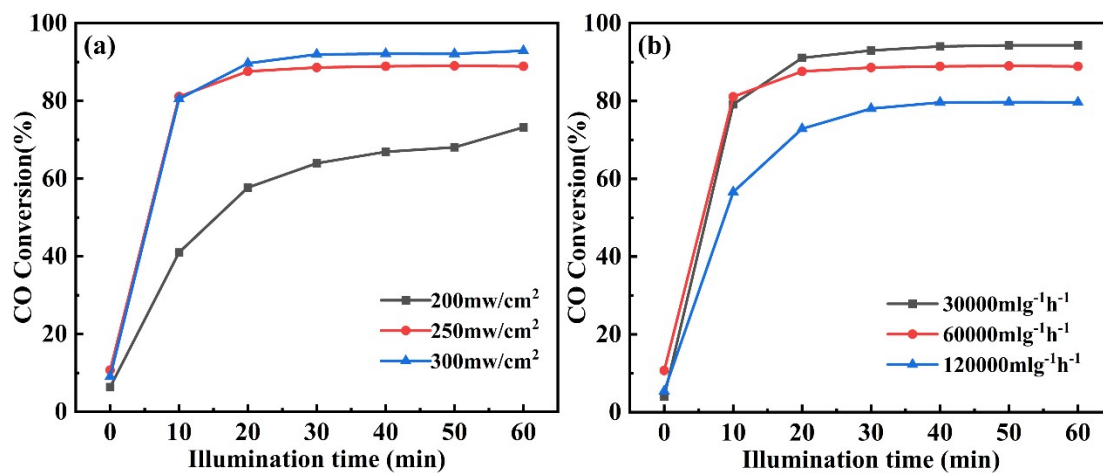


Figure S8. CO conversion of CuCoMnO_x-300 in CO-PROX at different illumination power densities (a) and at different weight hourly space velocity (b) at 250 mW/cm² (b).

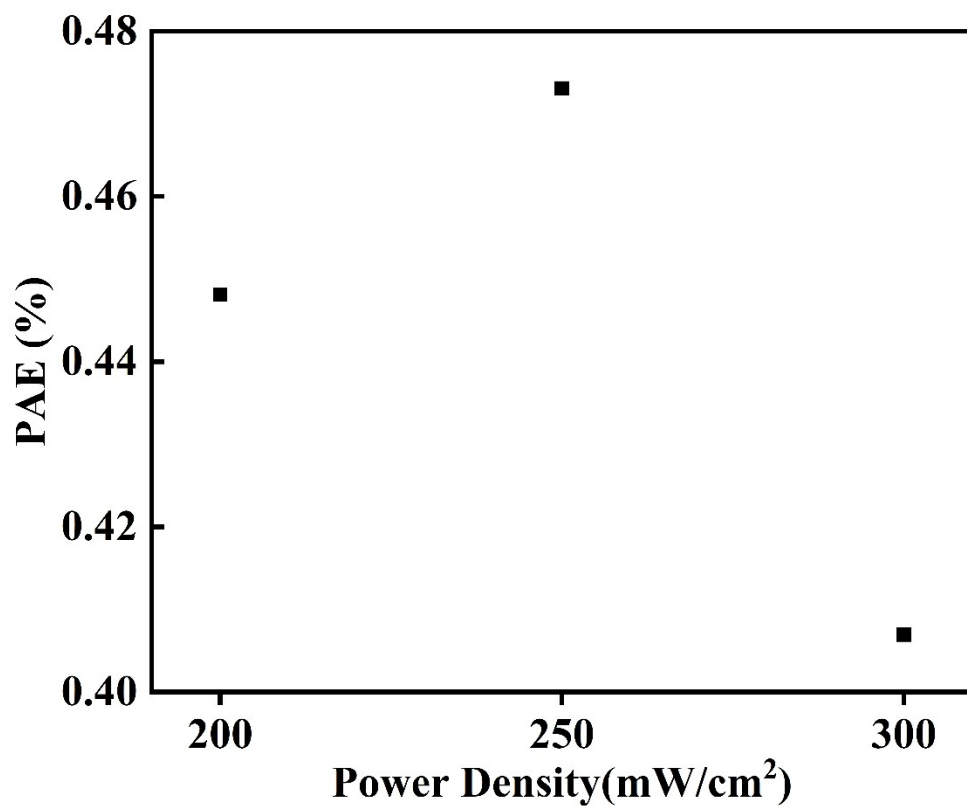


Figure S9. PAE values of CuCoMnO_x-300 catalyst under different illumination densities.

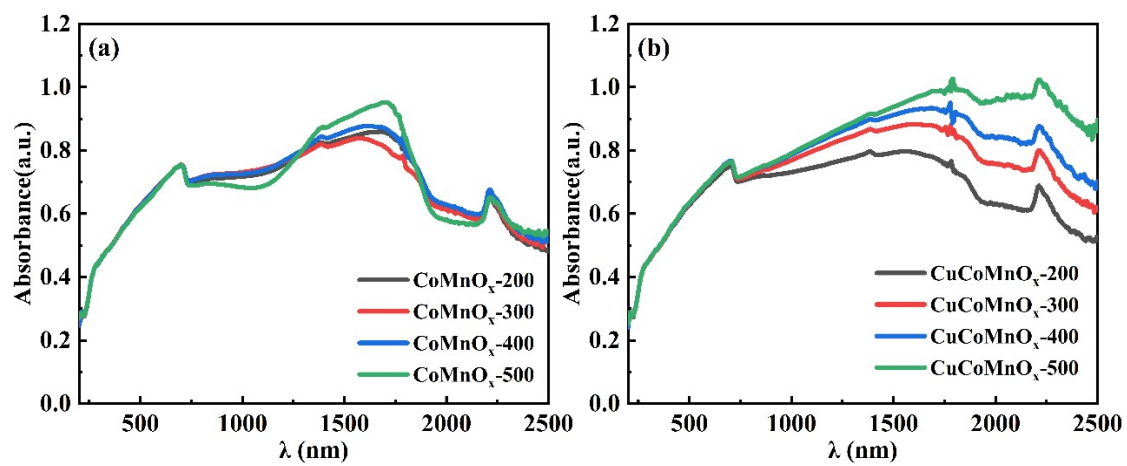


Figure S10. UV-Vis-IR absorption spectrums of (a) CoMnO_x -T, (b) CuCoMnO_x -T.

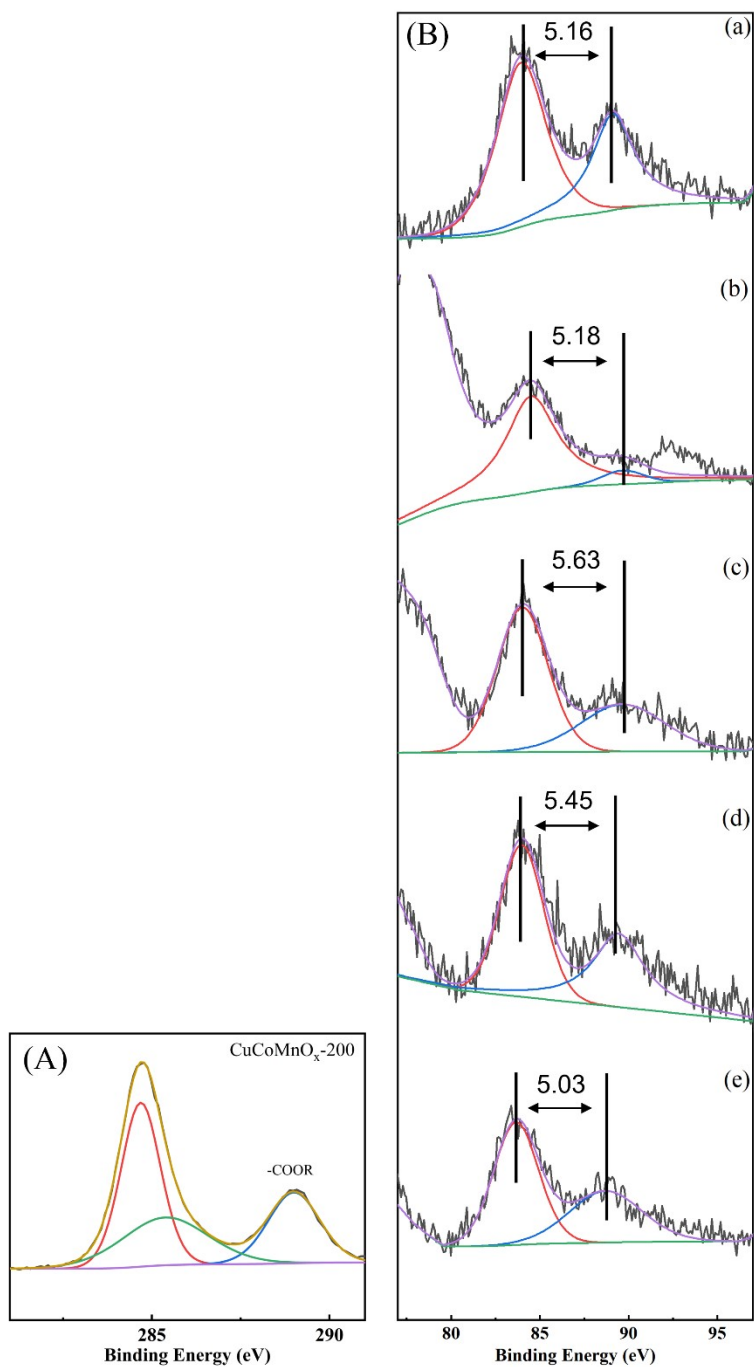


Figure S11. XPS spectra of C 1s (A) and Mn 3s (B) of CoMnO_x-300 (a), CuCoMnO_x-200 (b), CuCoMnO_x-300 (c), CuCoMnO_x-400 (d) and CuCoMnO_x-500 (e).

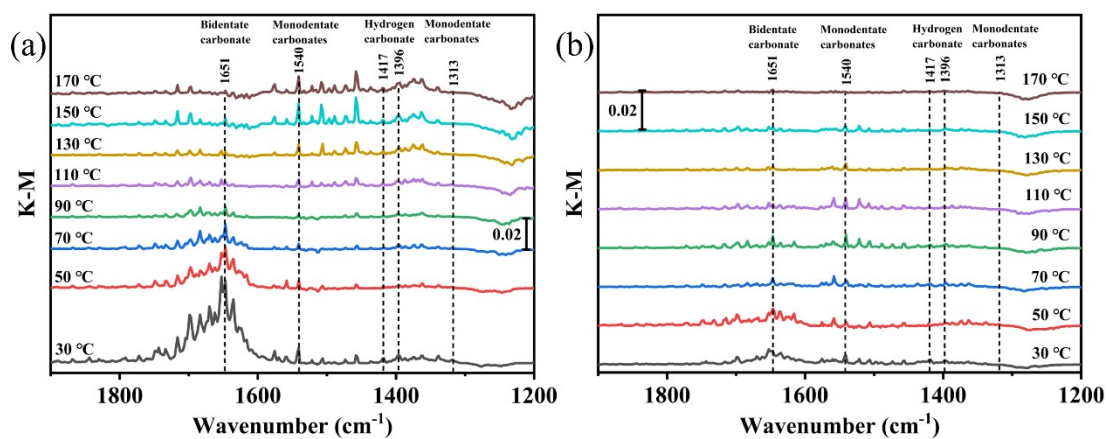


Figure S12. DRIFTS spectra (1900-1200 cm⁻¹) of CoMnO_x-300 (a) and CuCoMnO_x-300 (b) under the reaction stream at different temperature.

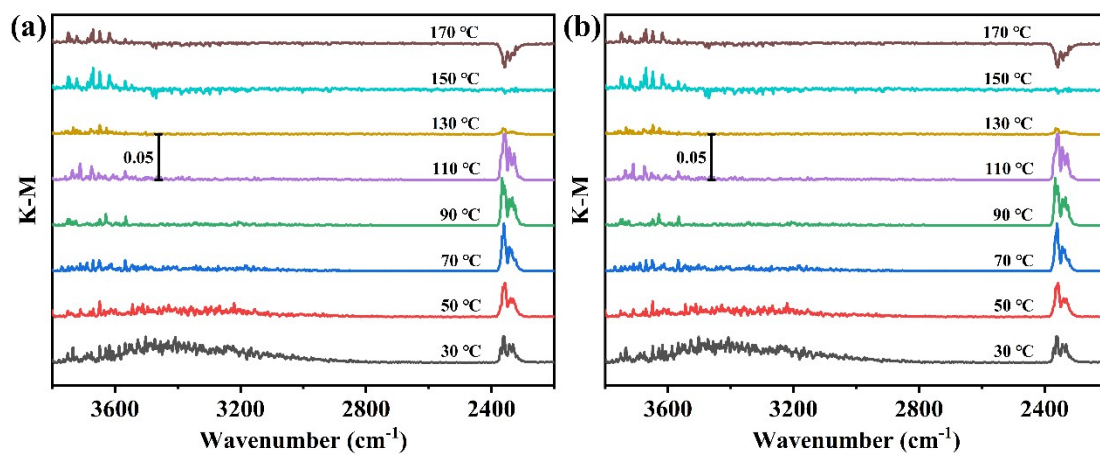


Figure S13. DRIFTS spectra (3800-2200 cm^{-1}) of $\text{CoMnO}_x\text{-300}$ (a) and $\text{CuCoMnO}_x\text{-300}$ (b).